NURBS-based isogeometric analysis of laminated composite beams using refined sinus model

M. Lezgy-Nazargah, P. Vidal, O. Polit

NURBS-based isogeometric analysis of laminated composite beams using refined sinus model

M. Lezgy-Nazargah [a], P. Vidal [b, *], O. Polit [b]

[a] Faculty of Civil Engineering, Hakim Sabzevari University, Sabzevar, Iran
[b] LEME — EA 4416, Université Paris Ouest, 50 rue de Sèvres, 92410 Ville d'Avray, France

A B S T R A C T

An isogeometric formulation based on non-uniform rational B-spline (NURBS) basis functions is presented for the analysis of laminated composite beams. A refined sinus model is considered in deriving the governing equations using the principle of virtual work. This refined sinus model does not require shear correction factor and ensures continuity conditions for displacements, transverse shear stresses as well as boundary conditions on the upper and lower surfaces of the laminated beam. It is important to notice that the number of the mechanical unknowns is independent of the number of layers. The proposed isogeometric finite element does not suffer from shear locking. Both static and vibration mechanical tests for thin and thick laminate beams are presented in order to validate the capability of the proposed isogeometric formulation. For different boundary conditions, fiber orientations and lay-up number, excellent agreement is found between the results obtained from the present formulation and reference results from open literature or finite element reference solutions.

1. Introduction

Due to their high specific strength and stiffness to weight ratios, laminated composite structures have been widely used in a wide range of engineering structures and modern industries. In order to avoid local failure phenomena such as delamination, matrix breakage, and local excessive plastic deformations, local variations of the stress distribution in the composite structures have to be determined accurately. Consequently, choosing an adequate mathematical model to accurately predict the local behaviors and performances of the mentioned structures under various environments is a key issue. According to published researches, various theories have been developed for composite or sandwich structures. The most accurate approach to analyze the laminated plates/beams is solving the governing differential equations of the three-dimensional (3D) elasticity (Pagano, 1969, 1970; Pagano and Hatfield, 1972). However, development of these solutions is a difficult task and the resulted solution cannot be expressed in a closed form for the general case of arbitrary geometry, boundary and loading conditions. These drawbacks encouraged some researchers to employ the two-dimensional (2D) models, prescribing variations of the displacement components in the transverse direction. Until now, many 2D theories have been introduced by researchers for the analysis of laminated structures. In 2D equivalent single layer theories (ESLTs), the number of the unknowns is independent of the number of layers. But, the transverse shear stress continuity in the interfaces of the layers is not guaranteed. Thus, in some circumstances, classical (Stavsky and Loewy, 1971), Reissner–Mindlin-type, first-order shear-deformation (FSDT) (Reissner, 1945; Mindlin, 1951), and third-order shear deformation (Whitney, 1969a) theories which are variants of the ESLT, may lead to inaccurate results. In order to overcome the drawbacks of the ESLT, the LayerWise (LWT) or discrete-layer theories were presented by some researchers (Reddy, 2004, 1987; Reddy et al., 1989; Barbero et al., 1990; Robbins and Reddy, 1993). The displacement field along the thickness of each ply is approximated by a piecewise continuous function. Nevertheless, the number of unknowns is dependent on the number of the layers which in turn, increases the computational cost. In order to improve the accuracy of the results and reduce the number of the unknowns for the multilayered composites, zigzag (ZZ) theories were proposed by some researchers. These theories are able to reproduce piecewise continuous displacement and transverse stress fields in the thickness direction of the laminated structures (Lekhnitskii, 1935; Ren, 1986; Ren and Owen, 1989; Ambartsumian, 1969; Whitney, 1969b; Icardi,

* Corresponding author.
E-mail addresses: m.lezgy@hsu.ac.ir (M. Lezgy-Nazargah), philippe.vidal@u-paris10.fr (P. Vidal), olivier.polit@u-paris10.fr (O. Polit).

1998, 2001a, 2001b; Reissner, 1986; Murakami, 1984, 1986; Carrera, 1999; Carrera, 2000). The 2D global–local higher-order plate theories (Li and Liu, 1997; Shariyat, 2010a, 2010b, 2010c; Lezgy-Nazargah et al., 2011; Beheshti-Aval and Lezgy-Nazargah, 2012, 2013; Beheshti-Aval et al., 2013) are also capable of giving accurate results. For a comprehensive overview on theories and computational models for laminated composite structures, readers can refer to Carrera and Brischetto (2009), Zhang and Yang (2009), and Hu et al. (2008).

In the literature, different analytical (Pagano, 1969, 1970; Pagano and Hatfield, 1972; Srinivas et al., 1970; Srinivas and Rao, 1970; Jiarang and Jianqiao, 1990; Vel and Batra, 1999; Leissa and Kang, 2002; Kang and Shim, 2004) and numerical approaches have been introduced for the analysis of laminated composite structures. The finite element method (Shariyat, 2010a, 2010b, 2010c; Lezgy-Nazargah et al., 2011; Beheshti-Aval and Lezgy-Nazargah, 2012, 2013; Beheshti-Aval et al., 2013), the finite difference method (Numayr et al., 2004; Wu et al., 2008), the meshfree methods (Bui et al., 2011), the differential quadrature methods (Alibeigloo and Madoliat, 2009), the Ritz methods (Liew, 1996; Venini and Mariani, 1997; Hu et al., 2004; Chen et al., 1997), the strip element method (Wang et al., 2001, 2000), etc. are also some of typical numerical methods which were successfully applied for the analysis of laminated composite structures. Among these methods, the finite element approach is one of the most powerful and reliable approaches for solving such problems. However, it has some inherent drawbacks due to the use of the so-called meshing process for obtaining a discretized geometry. This process often leads to geometrical errors. Moreover, mesh generation, re-meshing and achieving the smoothness with arbitrary continuity order between the elements are the cumbersome tasks and time-consuming procedures in the traditional finite element analysis. To overcome these drawbacks, a new powerful computational method, the so-called isogeometric approach, is recently introduced by Hughes et al. (2005). The conventional NURBS-based Computer Aided Design (CAD) tool is directly integrated into the finite element analysis. Indeed, isogeometric approach tries to overcome the gap between CAD and finite element analysis. Therefore, the same geometric definition of non-uniform rational B-spline basic functions is used to represent the field variable approximations of the structures as well as the geometry of structure. Isogeometric analysis based on NURBS basic functions can preserve exact geometries and enhance the accuracy of the traditional finite elements significantly. As well known, the NURBS basic functions can provide higher continuity of derivatives than that of Lagrange and Hermite interpolation functions that has been widely used in finite element formulation. In addition, the order of NURBS basic functions can be easily increased without changing the geometry or its parameterization (Rogers, 2001). Thanks to these features, isogeometric analysis has been used for solving different solid and fluid mechanics problems (Bazilevs and Hughes, 2008; Bazilevs et al., 2008; Wall et al., 2008; Qian, 2010; Verhoosel et al., 2011; Cottrell et al., 2006; Elguedj et al., 2008). However, few works are available in the literature which employ the isogeometric formulations for the analysis of laminated composite structures based on the advanced and refined theories. Thai et al. (2013) developed an isogeometric finite element method for static, free vibration and buckling analysis of laminated composite and sandwich plates based upon layer-wise theory. Shojaee et al. (2012) have introduced an isogeometric finite element formulation for natural frequencies and buckling analysis of thin symmetrically laminated composite plates based upon the classical plate theory (CPT). Kapoor and Kapania (2012) developed geometrically nonlinear NURBS isogeometric formulations for the bending analysis of laminated composite plates in conjunction with first-order shear-deformable theory. Thai Chien et al. (2012) studied free vibration and buckling problem of laminated composite Reissner–Mindlin plates using isogeometric analysis. Benson et al. (2010) studied Reissner–Mindlin shell problems using isogeometric analysis.

In the present study, an isogeometric approach for the development of a new beam element based on a refined sinus model is introduced for static and free vibration of laminated composite and sandwich beams. The employed refined sinus model is computationally low cost, efficient and simple to use. This sinus model was introduced first by Touratier (1991). Then, it was extended to take into account the interlaminar continuity of the transverse shear stresses by Polit and Touratier (2000) for plates, and by Dau et al. (2004) for shells. The original sinus model has been enriched by Vidal and Polit (2008) by introducing a layer refinement in the kinematics, and then extended to thermal and piezoelectric effects (Vidal and Polit, 2009; Beheshti-Aval et al., 2011; Beheshti-Aval and Lezgy-Nazargah, 2010; Lezgy-Nazargah et al., 2013). In this framework, this study is focused on the integrating of these last works into the isogeometric analysis. The NURBS basic functions are used to represent both geometric and field variable approximations. The accuracy and the effectiveness of the proposed method are justified through several numerical examples. The numerical results exhibit good agreements with the available published finite element results.

2. Formulation of the mechanical problem

2.1. Geometry, coordinate system

The laminated beam of length L has a rectangular uniform cross section, width b, height h, and is made of NC layers. The geometric parameters and the chosen Cartesian coordinate system (x_1, x_2, x_3) are shown in Fig. 1. The slenderness ratio is defined as $S = L/h$.

2.2. Constitutive equations

The 3D linear constitutive equations of the kth layer in its global material coordinate system can be expressed as:

$$\begin{Bmatrix} \sigma_{11}^{(k)} \\ \sigma_{22}^{(k)} \\ \sigma_{33}^{(k)} \\ \sigma_{23}^{(k)} \\ \sigma_{13}^{(k)} \\ \sigma_{12}^{(k)} \end{Bmatrix} = \begin{bmatrix} c_{11}^{(k)} & c_{12}^{(k)} & c_{13}^{(k)} & 0 & 0 & c_{16}^{(k)} \\ c_{12}^{(k)} & c_{22}^{(k)} & c_{23}^{(k)} & 0 & 0 & c_{26}^{(k)} \\ c_{13}^{(k)} & c_{23}^{(k)} & c_{33}^{(k)} & 0 & 0 & c_{36}^{(k)} \\ 0 & 0 & 0 & c_{44}^{(k)} & c_{45}^{(k)} & 0 \\ 0 & 0 & 0 & c_{45}^{(k)} & c_{55}^{(k)} & 0 \\ c_{16}^{(k)} & c_{26}^{(k)} & c_{36}^{(k)} & 0 & 0 & c_{66}^{(k)} \end{bmatrix} \begin{Bmatrix} \varepsilon_{11}^{(k)} \\ \varepsilon_{22}^{(k)} \\ \varepsilon_{33}^{(k)} \\ 2\varepsilon_{23}^{(k)} \\ 2\varepsilon_{13}^{(k)} \\ 2\varepsilon_{12}^{(k)} \end{Bmatrix} \tag{1}$$

where σ_{ij} and ε_{ij} denote the stress and the infinitesimal strain tensor components respectively. c_{kl} are the elastic material constants. In a laminated composite beam with small width, the

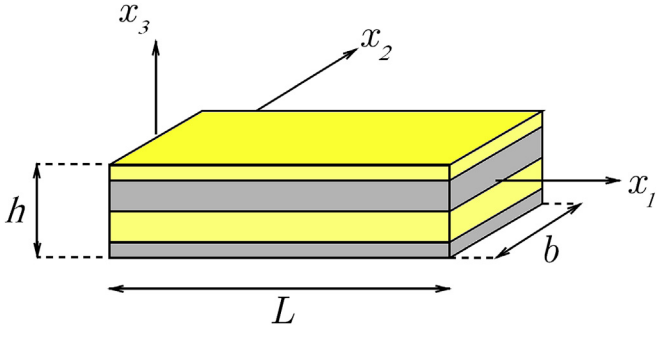

Fig. 1. Laminated composite beam: Cartesian coordinate system and geometric parameters.

introduction of the classical plane stress conditions leads to the 1D constitutive relation (2):

$$\overline{\boldsymbol{\sigma}} = \overline{\mathbf{C}}\overline{\boldsymbol{\varepsilon}} \tag{2}$$

where

$$\overline{\boldsymbol{\sigma}} = \begin{bmatrix} \sigma_{11}^{(k)} \\ \sigma_{13}^{(k)} \end{bmatrix}, \quad \overline{\boldsymbol{\varepsilon}} = \begin{bmatrix} \varepsilon_{11}^{(k)} \\ 2\varepsilon_{13}^{(k)} \end{bmatrix}$$

$$\overline{\mathbf{C}} = \begin{bmatrix} c_{11}^{(k)} & 0 \\ 0 & c_{55}^{(k)} \end{bmatrix} - \begin{bmatrix} c_{12}^{(k)} & c_{13}^{(k)} & c_{16}^{(k)} & 0 \\ 0 & 0 & 0 & c_{45}^{(k)} \end{bmatrix} \begin{bmatrix} c_{22}^{(k)} & c_{23}^{(k)} & c_{26}^{(k)} & 0 \\ c_{23}^{(k)} & c_{33}^{(k)} & c_{36}^{(k)} & 0 \\ c_{26}^{(k)} & c_{36}^{(k)} & c_{66}^{(k)} & 0 \\ 0 & 0 & 0 & c_{44}^{(k)} \end{bmatrix}^{-1} \begin{bmatrix} c_{12}^{(k)} & 0 \\ c_{13}^{(k)} & 0 \\ c_{16}^{(k)} & 0 \\ 0 & c_{45}^{(k)} \end{bmatrix}$$

2.3. Weak formulation

The governing equations of motion are derived based on the principle of virtual work. This principle for a laminated composite structure on a volume Ω and regular boundary surface Γ can be written as follows. We search the displacement such that

$$\begin{aligned} \delta\Pi &= \delta U - \delta W \\ &= -\int_{\Omega} \boldsymbol{\delta\varepsilon}^T \boldsymbol{\sigma}\, d\Omega + \int_{\Gamma} \boldsymbol{\delta u}^T \mathbf{F}_S\, d\Gamma + \int_{\Omega} \boldsymbol{\delta u}^T \mathbf{F}_V\, d\Omega - \int_{\Omega} \rho \boldsymbol{\delta u}^T \ddot{\mathbf{u}}\, d\Omega = 0 \end{aligned} \tag{3}$$

where $\mathbf{F}_S$, $\mathbf{F_V}$, and ρ are surface force vector, mechanical body force vector and mass density, respectively. $\delta\mathbf{u}$ denote admissible virtual displacements.

2.4. Displacement and strain fields

The displacement field used in the present study is given by Vidal and Polit (2008):

$$\begin{aligned} u_1(x_1,x_2,x_3,t) = u(x_1,t) - x_3 w(x_1,t)_{,1} + \left(\omega_3(x_1,t) + w(x_1,t)_{,1}\right) \\ \times F(x_3) + S(x_3) u_{31}^1(x_1,t) \end{aligned} \tag{4}$$

$$u_3(x_1,x_2,x_3,t) = w(x_1,t)$$

where the functions $u_1(x_1,x_2,x_3,t)$ and $u_3(x_1,x_2,x_3,t)$ represent the axial and transverse displacement components, respectively. t is the time $u(x_1,t)$ and $w(x_1,t)$ are the displacement components of the central line. $\omega_3(x_1,t)$ denotes the shear-bending rotation around the x_2 axis. $u_{31}^1(x_1,t)$ is an additional unknown function associated with the refinement per layer. In the context of the refined sinus model, we also have:

$$\begin{aligned} F(x_3) = \frac{h}{\pi}\sin\left(\frac{\pi x_3}{h}\right) + \sum_{k=1}^{NC} \Bigg(\overline{z}_k \beta_1^k + \left(-\frac{1}{2} + \frac{3\overline{z}_k^2}{2}\right)\beta_2^k \\ + \left(-\frac{3\overline{z}_k}{2} + \frac{5\overline{z}_k^3}{2}\right)\beta_3^k \Bigg) \left(H(x_3 - z_k) - H(x_3 - z_{k+1})\right) \end{aligned}$$

$$\begin{aligned} S(x_3) = \sum_{k=1}^{NC} \Bigg(\overline{z}_k \delta_1^k + \left(-\frac{1}{2} + \frac{3\overline{z}_k^2}{2}\right)\delta_2^k + \left(-\frac{3\overline{z}_k}{2} + \frac{5\overline{z}_k^3}{2}\right)\delta_3^k \Bigg) \\ \times \left(H(x_3 - z_k) - H(x_3 - z_{k+1})\right) \end{aligned} \tag{5}$$

where $\overline{z}_k = a_k x_3 - b_k$, $a_k = \frac{2}{z_{k+1} - z_k}$, $b_k = \frac{z_{k+1} + z_k}{z_{k+1} - z_k}$ with $x_3 \in [z_k; z_{k+1}]$.

In the above equations, H is the Heaviside's function. $\beta_1^k, \beta_2^k, \beta_3^k, \delta_1^k, \delta_2^k$ and δ_3^k are coefficients deduced from the inter-laminar continuity conditions of the transverse shear stress on the interfaces between the layers, and the boundary conditions on the upper and lower surfaces of the beam. It is worthy to note that these coefficients depend only on the material properties and the global coordinates of the layers. It is seen from Eqs. (6)–(7) that the refined sinus model includes only four mechanical generalized unknowns u, w, ω_3 and u_{31}^1. For further details on the formulations, the interested readers can refer to Vidal and Polit (2008).

The strain equations can be derived from the displacement field:

$$\begin{aligned} \varepsilon_{11} &= u_{,1} - (x_3) w_{,11} + \left(\omega_{3,1} + w_{,11}\right) F(x_3) + S(x_3) u_{31,1}^1 \\ \gamma_{13} &= 2\varepsilon_{13} = \left(\omega_3 + w_{,1}\right) F(x_3)_{,3} + S(x_3)_{,3} u_{31}^1 \end{aligned} \tag{6}$$

3. Isogeometric approximation

3.1. NURBS basis functions

NURBS curves are constructed by taking a linear combination of NURBS basis functions. The coefficients of the basis functions are referred to as control points. These are somewhat analogous to nodal points in the traditional finite element analysis. Piecewise linear interpolation of the control points gives the so-called control polygon. A NURBS curve of order k−1 is defined as:

$$P(\xi) = \sum_{i=1}^{n+1} B_i R_{i,k}(\xi) \quad , \xi_{\min} \le \xi < \xi_{\max}, 2 \le k \le n+1 \tag{7}$$

where B_i are the coordinate position of $n+1$ control points and $R_{i,k}(\xi)$ are the NURBS basis functions which are defined as:

$$R_{i,k}(\xi) = \frac{h_i N_{i,k}(\xi)}{\sum_{i=1}^{n+1} h_i N_{i,k}(\xi)} \tag{8}$$

where h_i are a set of $n+1$ homogenous weighting factors corresponding to the control points and $N_{i,k}$ represents the ith normalized B-spline basis functions of order k−1 which are defined by the following Cox-de Boor recursion formulas (Rogers, 2001):

$$N_{i,1}(\xi) = \begin{cases} 1 & \text{if } \xi_i \le \xi < \xi_{i+1} \\ 0 & \text{otherwise} \end{cases} \tag{9-a}$$

$$N_{i,k}(\xi) = \frac{(\xi - \xi_i)N_{i,k-1}(\xi)}{\xi_{i+k-1} - \xi_i} + \frac{(\xi_{i+k} - \xi)N_{i+1,k-1}(\xi)}{\xi_{i+k} - \xi_{i+1}} \tag{9-b}$$

The values of ξ_i are elements of a knot vector satisfying the relation $\xi_i \le \xi_{i+1}$. A knot vector in one dimension is a set of coordinates in the parametric space, written $\Xi = \{\xi_1, \xi_2, ..., \xi_{n+k+1}\}$, where is $\xi_i \in \Re$. Knots divide the parametric space into knot spans or elements. They are somewhat analogous to elements in the traditional finite element analysis. Fundamentally, two types of knot vector are used, periodic and open, in two manners, uniform and non-uniform. If knots are equally-spaced in the parametric space, they are said to be uniform. If they are unequally spaced, they are non-uniform. More than one knot can be located at the same coordinate in the parametric space. These are referred to as repeated knots. An open knot vector has multiplicity of knot values at the ends equal to k. In the isogeometric analysis, with the purpose of satisfying the Kronecker delta property at boundary points, an open knot vector, i.e., a knot vector with k repeated knots at the ends, is used (Roh and Cho, 2004). In one dimension, basis functions formed from open knot vectors are interpolatory at the ends of the parametric space interval, $\{\xi_1, \xi_{n+k+1}\}$, but they are not, in general, interpolatory at interior knots. This is a distinguishing feature between knots and "nodes" in finite element analysis.

The important properties of the NURBS basis functions can also be summarized as follows:

(1) They are polynomial of degree k−1 on each interval $\xi_i \le \xi < \xi_{i+1}$.
(2) They have continuous derivatives of degree k−2 in the absence of repeated knots or control points.
(3) Repeating a knot or control point m times decreases the number of continuous derivatives by m.

It is worthy to note that what we refer to as "order" in the usual terminology in the finite element literature, is usually referred to as "degree" in the computational geometry literature. For more details about NURBS basis functions, readers can refer to Rogers (2001).

3.2. Approximation of the boundary value problem

In this section, the NURBS basis function is employed for both the parameterization of the geometry and the approximation of the mechanical variables of Eq. (4) as follow:

$$\begin{aligned} x_1(\xi) &= \sum_{i=1}^{n+1} \tilde{x}_i R_{i,k}(\xi) \\ u(x_1(\xi)) &= \sum_{i=1}^{n+1} \tilde{u}_i R_{i,k}(\xi), \quad w(x_1(\xi)) = \sum_{i=1}^{n+1} \tilde{w}_i R_{i,k}(\xi) \\ \omega_3(x_1(\xi)) &= \sum_{i=1}^{n+1} \tilde{\omega}_{3i} R_{i,k}(\xi), \quad u^1_{31}(x_1(\xi)) = \sum_{i=1}^{n+1} \tilde{u}^1_{31i} R_{i,k}(\xi) \end{aligned} \tag{10}$$

In Eq. (10), ξ is the parametric coordinate, $x_1(\xi)$ is the physical coordinate, $\tilde{x}_i$ represents the physical coordinate position of ith control point of an $n+1$ control mesh. $\tilde{u}_i, \tilde{w}_i, \tilde{\omega}_3$ and $\tilde{u}^1_{31i}$ represents the values of the unknown displacement variables u, w, ω_3 and u^1_{31} at each control point (control variables), respectively. $R_{i,k}(\xi)$ denote the NURBS basis functions of order $k-1$.

Based on Eqs. (4) and (6), displacements and strain components can be expressed under the following matrices form:

$$\{\mathbf{u}\} = [\mathbf{A}]\{\mathbf{u_u}\} \quad , \quad \{\varepsilon\} = [\mathbf{L}]\{\mathbf{u_u}\} \tag{11}$$

where $\mathbf{u} = [u_1 \quad u_3]^T$, $\mathbf{u}_u = \begin{bmatrix} u & w & \omega_3 & u^1_{31} \end{bmatrix}^T$, $\varepsilon = [\varepsilon_{11} \quad \gamma_{13}]^T$, and

$$\mathbf{A} = \begin{bmatrix} 1 & -x_3\dfrac{d}{dx_1} + F(x_3)\dfrac{d}{dx_1} & F(x_3) & S(x_3) \\ 0 & 1 & 0 & 0 \end{bmatrix},$$

$$\mathbf{L} = \begin{bmatrix} \dfrac{d}{dx_1} & -x_3\dfrac{d^2}{dx_1^2} + F(x_3)\dfrac{d^2}{dx_1^2} & F(x_3)\dfrac{d}{dx_1} & S(x_3)\dfrac{d}{dx_1} \\ 0 & F(x_3)_{,3}\dfrac{d}{dx_1} & F(x_3)_{,3} & S(x_3)_{,3} \end{bmatrix}$$

Using Eq. (10), the vector of displacement components $\mathbf{u}_u$ may be expressed in terms of the unknown control variables $\tilde{\mathbf{u}}_u$ as follows:

$$\{\mathbf{u_u}\} = [\mathbf{R}]\{\tilde{\mathbf{u}}_u\} \tag{12}$$

where

$$\tilde{\mathbf{u}}_u = \left\{ \tilde{u}_1 \quad \tilde{u}_2 \quad \cdots \quad \tilde{u}_{n+1} \vdots \quad \tilde{w}_1 \quad \tilde{w}_2 \quad \cdots \quad \tilde{w}_{n+1} \vdots \quad (\tilde{\omega}_3)_1 \quad (\tilde{\omega}_3)_2 \quad \cdots \quad (\tilde{\omega}_3)_{n+1} \vdots \quad \left(\tilde{u}^1_{31}\right)_1 \quad \left(\tilde{u}^1_{31}\right)_2 \quad \cdots \quad \left(\tilde{u}^1_{31}\right)_{n+1} \right\}^T$$

$$\mathbf{R} = \begin{bmatrix} R_{i,1} & R_{i,2} & \cdots & R_{i,n+1} & 0 & 0 & \cdots & 0 & 0 & 0 & \cdots & 0 & 0 & 0 & \cdots & 0 \\ 0 & 0 & \cdots & 0 & R_{i,1} & R_{i,2} & \cdots & R_{i,n+1} & 0 & 0 & \cdots & 0 & 0 & 0 & \cdots & 0 \\ 0 & 0 & \cdots & 0 & 0 & 0 & \cdots & 0 & R_{i,1} & R_{i,2} & \cdots & R_{i,n+1} & 0 & 0 & \cdots & 0 \\ 0 & 0 & \cdots & 0 & 0 & 0 & \cdots & 0 & 0 & 0 & \cdots & 0 & R_{i,1} & R_{i,2} & \cdots & R_{i,n+1} \end{bmatrix}$$

Using Eqs. (11) and (12), the displacements and strain vectors can be expressed as follows:

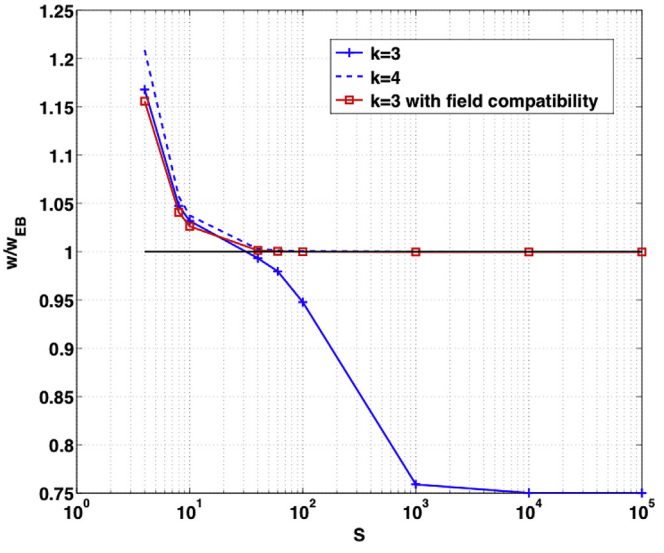

Fig. 2. Transverse displacement versus the aspect ratio for the cantilever beam (n = 7).

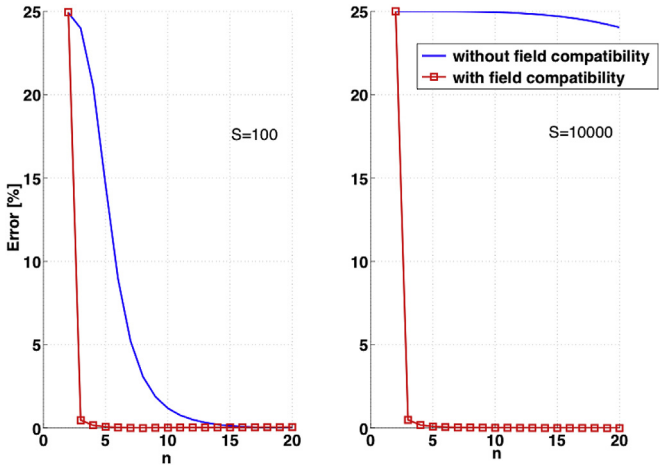

Fig. 3. Convergence of the transverse displacement of the cantilever beam for two values of length-to-thickness ratio; (k = 3).

$$\{\mathbf{u}\} = \mathscr{N}\{\tilde{\mathbf{u}}_u\} \quad , \quad \{\varepsilon\} = \mathscr{B}\{\tilde{\mathbf{u}}_u\} \tag{13}$$

with

$$\mathscr{N} = [\mathbf{A}][\mathbf{R}] \text{ and } \mathscr{B} = [\mathbf{L}][\mathbf{R}] \tag{14}$$

Substituting Eqs. (2) and (13) into Eq. (3), and assembling the elementary matrices yield the following dynamical discrete equation:

$$\mathbf{M}\ddot{q}(t) + \mathbf{K}\mathbf{q}(t) = \mathbf{F}(t) \tag{15}$$

where $\boldsymbol{q}$(t) denotes the vector of unknown displacement variables at the control points. The matrices and vectors in the above equation are the global mass matrix $\mathbf{M} = \int_{\Omega} \rho \mathscr{N}^T \mathscr{N}\, d\Omega$, the global stiffness matrix $\mathbf{K} = \int_{\Omega} \mathscr{B}^T \overline{\mathbf{C}}\, \mathscr{B}\, d\Omega$, and loads vector $\mathbf{F}(t) = \int_{\Omega} \mathscr{N}^T \mathbf{F_V}\, d\Omega + \int_{\Gamma} \mathscr{N}^T \mathbf{F_S}\, d\Gamma$.

4. Results and discussions

In the present section, static and free vibration analyses of isotropic, laminated composite and sandwich beams with different stacking sequences and boundary conditions are considered to evaluate the efficiency and the accuracy of the present isogeometric formulation. Results of the present formulation are compared with either previously published results of well-known references or with the finite element results obtained with commercial codes (ANSYS and ABAQUS solutions).

4.1. Static analysis

4.1.1. Shear locking

First, the shear locking phenomenon is addressed on an isotropic cantilever beam submitted to a point load. The material properties are such as E = 210000 MPa and ν = 0.3. Variations of the normalized deflection versus the aspect ratio are shown in Fig. 2. Comparison of the present results with results of the Euler–Bernoulli beam theory reveals that a shear locking occurs for the quadratic (k = 3) NURBS basis function. This phenomenon disappears for higher order functions (see Fig. 2 for k = 4) as it has already been shown in Echter and Bischoff (2010). Note that the approximation using the linear basis functions (k = 2) is not considered as it is the same one in the Finite Element method.

Nevertheless, the shear locking can be avoided using the field compatibility approach developed in Polit et al. (2012) and extended in the present work. For k = 3, it can be inferred from Fig. 2 that the shear locking is avoided using this methodology.

A convergence study using different values of n is also presented in Fig. 3 for S = 100 and S = 10^5 with respect to the Euler–Bernoulli solution. A comparison is given between the isogeometric approximation and the field compatibility methodology. For a thin plate (S = 10^5), the locking disappears. Moreover, the convergence rate is independent of the length to thickness ratio.

4.1.2. Properties of the isogeometric approach

In this section, a three-layered [0°/90°/0°] simply supported composite beam with various values of length to thickness ratio is analyzed using the proposed isogeometric formulation. The beam is made of carbon/epoxy with the following material properties:

$$(E_L, E_T, G_{LT}, G_{TT}) = (172.4, 6.895, 3.448, 1.379)GPa,$$
$$(\nu_{LT}, \nu_{TT}) = (0.25, 0.25)$$

L and T denote directions parallel and normal to the fibers, respectively. All layers of the beam have equal thickness. The beam is subjected to a sinusoidal pressure $p(x_1) = p_0 \sin(\pi x_1/L)$ on its top surface. Accuracy of the results of the present isogeometric formulation is assessed by comparing with those of Pagano (1969). This three-layered composite beam has been also studied by Vidal and Polit (2008) using refined sinus finite element model. The present results are also compared with this one. The following normalized quantities are used:

$$(\overline{u}_1, \overline{u}_3) = E_T\left(u_1/h\, p_0,\ 100u_3\Big/LS^3p_0\right),$$
$$(\overline{\sigma}_{11}, \overline{\tau}_{13}) = (\sigma_{11}, \tau_{13})/p_0$$

4.1.2.1. Convergence study. A convergence study varying the number of control points and for different orders of NURBS basis functions is carried out. Table 1 shows results of the convergence study using different orders of NURBS basis functions with the linear parameterization and a fixed number of control points/nodes

Table 1
Results of the convergence study for the three-layer [0°/90°/0°] beam using various orders of NURBS basis functions; n = 7; (S = 4).

	No. elements	No. dof	$\overline{u}_3(0.5L, 0)$	$\overline{u}_1(0, 0.5h)$	$\overline{\sigma}_{13}(0,0)$(C)	$\overline{\sigma}_{13}(0,0)$ (E)	$\overline{\sigma}_{11}(0.5L, 0.5h)$
k = 2	7	32	5.2589	2.5693	2.1778	0	14.10
k = 3	6	32	2.8841	0.9602	1.4913	0.6937	17.63
k = 4	5	32	2.9091	0.9439	1.4229	1.2861	18.17
k = 5	4	32	2.9097	0.9435	1.4212	1.5699	18.49
k = 6	3	32	2.9099	0.9437	1.4221	1.4869	18.51
k = 7	2	32	2.9101	0.9437	1.4220	1.4295	18.53
k = 8	1	32	2.9101	0.9437	1.4220	1.4326	18.53

Table 2
Results of the convergence study for the three-layer $[0^\circ/90^\circ/0^\circ]$ beam; various orders of NURBS basis functions versus different numbers of elements; ($S = 4$).

	No. elements	No. control points	No. dof	$\bar{u}_3(0.5L,\ 0)$	$\bar{u}_1(0, 0.5h)$	$\bar{\sigma}_{13}(0,0)$(C)	$\bar{\sigma}_{13}(0,0)$(E)	$\bar{\sigma}_{11}(0.5L, 0.5h)$
k = 3	2	3	12	2.7466	0.9996	1.6457	0.8645	18.44
	4	5	20	2.8483	0.9708	1.5339	0.5969	16.73
	8	9	36	2.8967	0.9555	1.4720	0.7748	18.09
	16	17	68	2.9077	0.9483	1.4420	0.9680	18.46
	32	33	132	2.9096	0.9456	1.4302	1.0625	18.51
k = 4	2	4	16	2.9091	0.9535	1.4628	0.8160	21.28
	4	6	24	2.9104	0.9440	1.4235	1.2000	19.61
	8	10	40	2.9102	0.9437	1.4222	1.3751	18.79
	16	18	72	2.9101	0.9437	1.4219	1.4201	18.50
	32	34	136	2.9101	0.9437	1.4219	1.4299	18.53
k = 5	2	5	20	2.9071	0.9419	1.4141	1.5186	18.49
	4	7	28	2.9097	0.9435	1.4212	1.5699	18.49
	8	11	44	2.9101	0.9436	1.4219	1.4647	18.53
	16	19	76	2.9101	0.9437	1.4219	1.4341	18.53
	32	35	140	2.9101	0.9437	1.4219	1.4341	18.53
k = 7	2	7	28	2.9101	0.9437	1.4220	1.4295	18.53
	4	9	36	2.9101	0.9437	1.4219	1.4284	18.53
	8	13	52	2.9101	0.9437	1.4219	1.4325	18.53
	16	21	84	2.9101	0.9437	1.4219	1.4325	18.53
	32	37	148	2.9101	0.9437	1.4219	1.4325	18.53
Exact	–	–	–	2.8872	0.9396	1.4318	1.4318	18.8

Table 3
The coordinates of different sets of control points employed in the static tests.

i	1	2	3	4	5	6	7	8	
	0	$0.07L$	$0.20L$	$0.40L$	$0.60L$	$0.80L$	$0.93L$	L	Case a
$\tilde{x}_i$	0	$0.14L$	$0.28L$	$0.50L$	$0.64L$	$0.79L$	$0.86L$	L	Case b
	0	$0.26L$	$0.29L$	$0.43L$	$0.57L$	$0.71L$	$0.94L$	L	Case c
	0	$0.14L$	$0.28L$	$0.43L$	$0.57L$	$0.71L$	$0.86L$	L	Case d

($n = 7$). Note that the transverse shear stress is calculated using two different methods: (i) employing the constitutive equations; (ii) integrating the elasticity equilibrium equations, along the thickness of laminates. Results of these two approaches are denoted by (C) and (E), respectively. It is seen that the displacement components are less sensitive to the orders of NURBS basis functions than the stress components and the convergence velocity is high.

Different numbers of elements are also considered with a fixed expansion order for the NURBS basis functions. Results are summarized in Table 2. In this table, the number of degrees of freedom are also given. It should be noticed that the convergence rate is better for the higher order expansion of NURBS basis functions. Considering the number of dofs, the use of k = 7 with two elements is suitable for the static analysis and drives to only 32 dofs. This is much lower than the corresponding results with classical FE approach (136 dofs). It can be also mentioned that the order of NURBS basis functions can be increased without increasing the number of nodes. This property is an advantage of the isogeometric analysis.

4.1.2.2. Influence of the parameterization. Different parameterizations can be used for the geometry and the sensitivity of the results can be compared. To this end, the three-layered $[0^\circ/90^\circ/0^\circ]$ composite beam is modelized using cubic NURBS basis functions with different sets of control points. Data of different control points are given in Table 3. A linear parameterization (case a) is compared with different non-linear ones (case b, c, d). The obtained bending numerical results are shown in Table 4. It can be observed that the

Table 4
The effect of different parameterization on the bending static results; three-layers $[0^\circ/90^\circ/0^\circ]$ beam with S = 4; (n = 7, k = 4).

	$\bar{u}_3(0.5L,\ 0)$	$\bar{u}_1(0, 0.5h)$	$\bar{\sigma}_{13}(0,0)$(C)	$\bar{\sigma}_{11}(0.5L, 0.5h)$
Case a	2.9091 (0.76%)	0.9439 (0.46%)	1.4229 (0.62%)	18.17 (3.35%)
Case b	2.8512 (1.25%)	0.9460 (0.68%)	1.4332 (0.10%)	19.85 (5.6%)
Case c	2.8925 (0.18%)	0.8645 (8.00%)	1.2122 (15.34%)	19.24 (2.33%)
Case d	2.9036 (0.57%)	0.9439 (0.46%)	1.42605 (0.40%)	18.38 (2.24%)

Table 5
The different sets of weighting factors corresponding to the control points considered for the three-layers $[0^\circ/90^\circ/0^\circ]$ beam with n = 7.

i	1	2	3	4	5	6	7	8	
$\tilde{x}_i$	0	$0.14L$	$0.28L$	$0.43L$	$0.57L$	$0.71L$	$0.86L$	L	
	1	1	1	1	1	1	1	1	Case 1
	1	1	1	2	2	1	1	1	Case 2
	1	1	1	1.5	1.5	1	1	1	Case 3
	1	1	1	0.75	0.75	1	1	1	Case 4
	1	1	1	0.5	0.5	1	1	1	Case 5
	1	1	1	1.5	1	1	1	1	Case 6
h_i	1	1	1.5	1	1	1.5	1	1	Case 7
	1	1.3	1.7	2	2	1.7	1.3	1	Case 8
	1	1.1	1.3	1.5	1.5	1.3	1.1	1	Case 9
	1.5	1.3	1.1	1	1	1.1	1.3	1.5	Case 10
	1	1	1	1	1	1.1	1.3	1.5	Case 11
	1	2	2	2	2	2	2	1	Case 12
	2	1	1	1	1	1	1	2	Case 13

Table 6
The effect of different weights of control points on the static bending results; three-layers $[0^\circ/90^\circ/0^\circ]$ beam with S = 4; (n = 7, k = 3).

	$\bar{u}_3(0.5L, 0)$	$\bar{u}_1(0, 0.5h)$	$\bar{\sigma}_{13}(0, 0)$ (C)	$\bar{\sigma}_{11}(0.5L, 0.5h)$
Case 1	2.8922 (0.17%)	0.9441 (0.48%)	1.4242 (0.53%)	17.90 (4.76%)
Case 2	2.6771 (7.28%)	0.8914 (5.13%)	1.3422 (6.26%)	18.57 (1.20%)
Case 3	2.8174 (2.42%)	0.9340 (0.60%)	1.4139 (1.25%)	18.30 (2.65%)
Case 4	2.8803 (0.24%)	0.9634 (2.53%)	1.5262 (6.59%)	17.48 (7.02%)
Case 5	2.8200 (2.33%)	0.9544 (1.58%)	1.5503 (8.28%)	18.25 (2.95%)
Case 6	2.8354 (1.79%)	0.9347 (0.52%)	1.4218 (0.70%)	15.84 (15.74%)
Case 7	2.6811 (7.14%)	0.8935 (4.91%)	1.3631 (4.80%)	13.56 (27.86%)
Case 8	2.7470 (4.86%)	0.9536 (1.49%)	1.5747 (9.98%)	15.51 (17.43%)
Case 9	2.8225 (2.24%)	0.9588 (2.04%)	1.5095 (5.43%)	16.33 (13.12%)
Case 10	2.9154 (0.98%)	0.9219 (1.88%)	1.3520 (5.57%)	19.17 (1.99%)
Case 11	2.9000 (0.44%)	0.9598 (2.15%)	1.4890 (3.99%)	19.74 (4.98%)
Case 12	2.2949 (20.51%)	0.7010 (25.39%)	1.2986 (9.30%)	15.75 (16.22%)
Case 13	2.4515 (15.09%)	0.6420 (31.67%)	0.6332 (55.78%)	15.34 (18.40%)

*The values in the parenthesis show the percent error.

Table 7
$\bar{u}_1(0, 0.5h)$ and $\bar{u}_3(0.5L, 0)$ for different values of S- three layer $[0°/90°/0°]$.

S	$\bar{u}_1(0, 0.5h)$				
	Present	Error (%)	SinRef-c	Error (%)	Exact
4	0.9437	0.4	0.9422	0.3	0.9396
20	67.0170	0.2	66.8640	<0.01	66.8696
40	519.28	0.2	518.08	<0.01	518.08
			$\bar{u}_3(0.5L, 0)$		
4	2.9101	0.8	2.9086	<1	2.8872
20	0.6187	0.2	0.6175	<0.1	0.6173
40	0.5380	0.2	0.5367	<0.01	0.5367

Table 8
$\bar{\sigma}_{13}(0, 0)$ for different values of S- three layer $[0°/90°/0°]$.

		$\bar{\sigma}_{13}(0, 0)$		
	S	4	20	40
Present	Direct (C)	1.4220	9.0093	18.215
	Error (%)	0.7	3.0	3.3
	Equil. eq (E)	1.4295	8.7418	17.588
	Error (%)	<1	<1	<1
SinRef-c	Direct (C)	1.4213	9.0052	18.184
	Error (%)	<1	2.9	3
	Equil. eq (E)	1.4236	8.6973	17.539
	Error (%)	<1	<1	<1
Exact		1.4318	8.7490	17.634

linear parameterization (case a) and the nonlinear parameterization with equally spaced control points (case d) give the most accurate results.

4.1.2.3. Influence of the weight. The effect of weights (Eq. (8)) of the control points on the accuracy of the numerical results is also studied. The control points and weights are given in Table 5. The associated results are shown in Table 6. We notice that the selection of non-equal weights for the control points increases the discrepancy between the isogeometric and elasticity results regardless of the weighting. Even if the distribution of the weights is symmetric, the accuracy of the results decreases.

Based on these results, the subsequent static results are calculated using equal weights for all control points, NURBS basis functions of order 6 (k = 7) with n = 7, and a linear parameterization of the geometry.

4.1.3. A simply supported three-layer $[0°/90°/0°]$ beam

The numerical results for deflection, in-plane displacements, transverse shear stress, and in-plane stress are given in Tables 7–9 for three different length to thickness ratios S = 4, 20, 40. In these Tables, the error of the present isogeometric analysis is compared with those obtained from the refined sinus finite element model (denoted SinRef-c) and exact reference solution. It is seen that the present isogeometric formulation has a good agreement with the exact solution. The accuracy of the present isogeometric formulation and refined sinus finite element (Vidal and Polit, 2008) are the same. The variation of normalized in-plane, inter-laminar shear

Table 9
$\bar{\sigma}_{11}(0.5L, 0.5h)$ for different values of S- three layer $[0°/90°/0°]$.

S	$\bar{\sigma}_{11}(0.5L, 0.5h)$				
	Present	Error (%)	SinRef-c	Error (%)	Exact
4	18.5	1.6	18.6	1	18.8
20	263.2	0	264.0	<0.5	263.2
40	1019.6	<0.02	1023.0	<0.5	1019.8

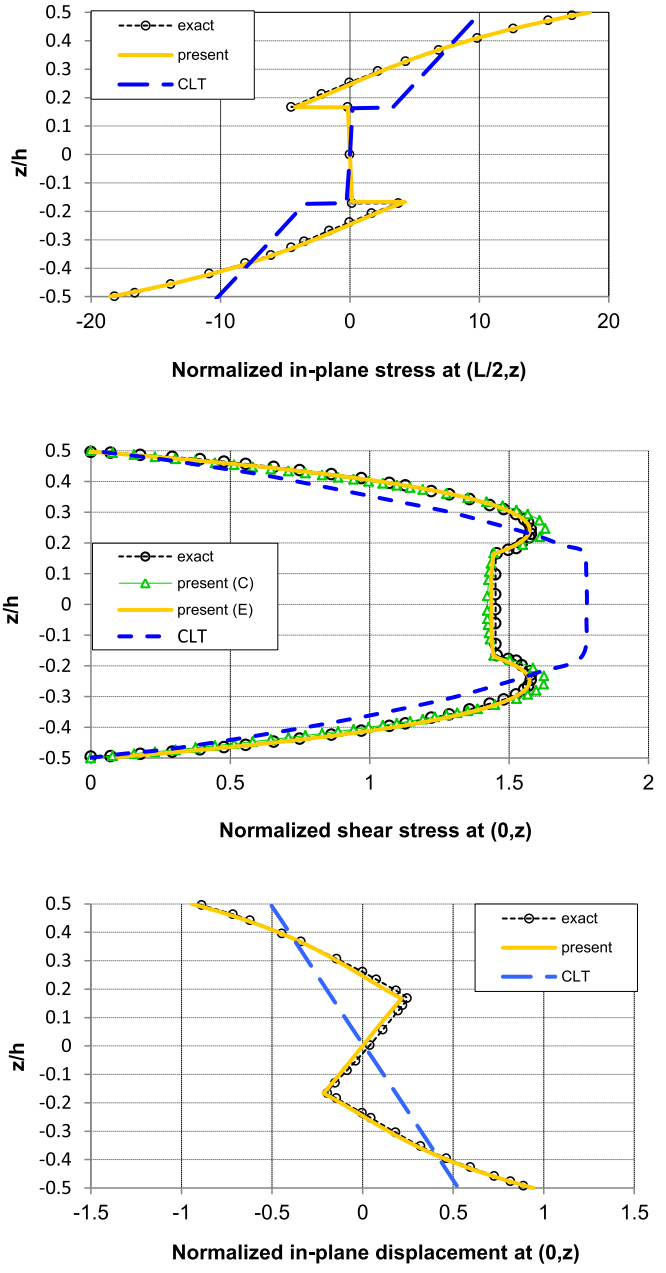

Fig. 4. Through-the-thickness distribution of $\bar{\sigma}_{11}$, $\bar{\sigma}_{13}$ and $\bar{u}_1$ for the simply supported three-layer beam ($S = 4$).

stresses and in-plane displacement through the thickness (S = 4) are presented in Fig. 4 for further comparison. In these figures, the present numerical results are also compared with the CLT's results (Pagano, 1969). Although the present laminated theory has only

Table 10
$\bar{u}_1(0, 0.5h)$ and $\bar{u}_3(0.5L, 0)$ for different values of S- two layer $[0°/90°]$.

S	$\bar{u}_1(0, 0.5h)$				
	Present	Error (%)	SinRef-c	Error (%)	Exact
4	4.80	5	4.78	5	4.55
20	487.54	0.5	486.20	0.2	485.15
40	3868.0	0.3	3858.7	<0.1	3856.3
			$\bar{u}_3(0.5L, 0)$		
4	4.7026	0.2	4.6964	<0.1	4.6950
20	2.7098	0.3	2.7035	<0.1	2.7027
40	2.6463	0.2	2.6400	<0.1	2.6398

Table 11
$\bar{\sigma}_{13}(0,-h/4)$ for different values of S- two layer $[0°/90°]$.

		$\bar{\sigma}_{13}(0,-h/4)$		
	S	4	20	40
Present	Direct (C)	2.589	13.494	27.136
	Error (%)	4	8	7
	Equil. eq (E)	2.788	14.604	29.095
	Error (%)	3	0.1	0.8
SinRef-c	Direct (C)	2.588	13.450	26.940
	Error (%)	4	8	8
	Equil. eq (E)	2.768	14.555	29.165
	Error (%)	2	0.5	0.5
Exact		2.706	14.620	29.324

Table 12
$\bar{\sigma}_{11}(L/2,-h/2)$ for different values of S- two layer $[0°/90°]$.

	$\bar{\sigma}_{11}(L/2,-h/2)$				
S	Present	Error (%)	SinRef-c	Error (%)	Exact
4	31.8	6	31.9	6	30.0
20	701.2	0.2	703.5	0.5	699.7
40	2793.5	0.03	2803.1	0.3	2792.6

two generalized unknowns more than CLT, the results are more accurate. It may be readily seen from Fig. 4 that the proposed isogeometric formulation predicts the in-plane stress very accurately. The transverse shear stress distribution obtained from the equilibrium equations is in better agreement with the exact solution. However, the presented isogeometric formulation predicts the transverse shear stress with sufficient accuracy from the constitutive law.

4.1.4. A simply supported two-layer $[0°/90°]$ beam

A two-layered $[0°/90°]$ simply supported composite beam with various values of length to thickness ratio is analyzed using the present isogeometric approach to evaluate the accuracy of the proposed formulation for an asymmetric lamination scheme with an extensional-bending coupling. Material properties and load conditions of the present example are the same as those of the previous one. The numerical results of this test case are also compared with both the refined sinus finite element models of Vidal and Polit (2008), CLT's results (Pagano, 1969), and 3D exact solution of Pagano (1969).

The results are summarized in Tables 10–12. Similar to the previous example, the present refined sinus isogeometric formulation is as accurate as the refined sinus finite element model. Fig. 5 depicts variations of the normalized in-plane displacement and stress components along the thickness direction. The transverse shear stress based on the equilibrium equations agrees very well with the exact elasticity solution. The proposed isogeometric approach also predicts the in-plane stress very accurately. Similar to the previous case, the accuracy of the transverse shear stress computed from the constitutive equations is satisfactory.

4.1.5. A four-layer cantilever beam with a symmetric lay-up

A four-layer cantilever beam with a length of $L = 10m$ and a unit width is analyzed using the isogeometric formulation for $S = 4,\ 10,$ and 50. The cantilever beam has a $[90°/0°/0°/90°]$ lamination scheme and its material properties are similar to those mentioned in section 4.1.2. The laminated beam is subjected to a distributed uniform pressure $p = 100N/m^2$ on its top surface. Since no exact 3D solution is available for the considered example, a 3D finite element analysis is performed in ABAQUS with a very refined mesh, using the 20-node C3D20R solid element.

For different values of the length to thickness ratio, the maximum transverse deflections are given in Table 13. The obtained results have a good agreement with results obtained from ABAQUS. It can be concluded from this table that the present isogeometric formulation predicts the deflection of the thin and thick laminated beams with an error rate of less than *2.35%*. To assess the accuracy of the present isogeometric formulation in predicting the local variations, distributions of the normalized in-plane displacement and stress across the thickness are depicted in Fig. 6 for the moderately thick beam ($S = 10$). These figures show that the proposed isogeometric formulation performs very well in the prediction of the transverse shear stress from the equilibrium equations. The maximum error in the case of moderately thick beam is approximately 3%. Concerning the transverse shear stress predicted from constitutive equations, the results are also good. It may easily seen from Fig. 6 that the depicted in-plane displacement is

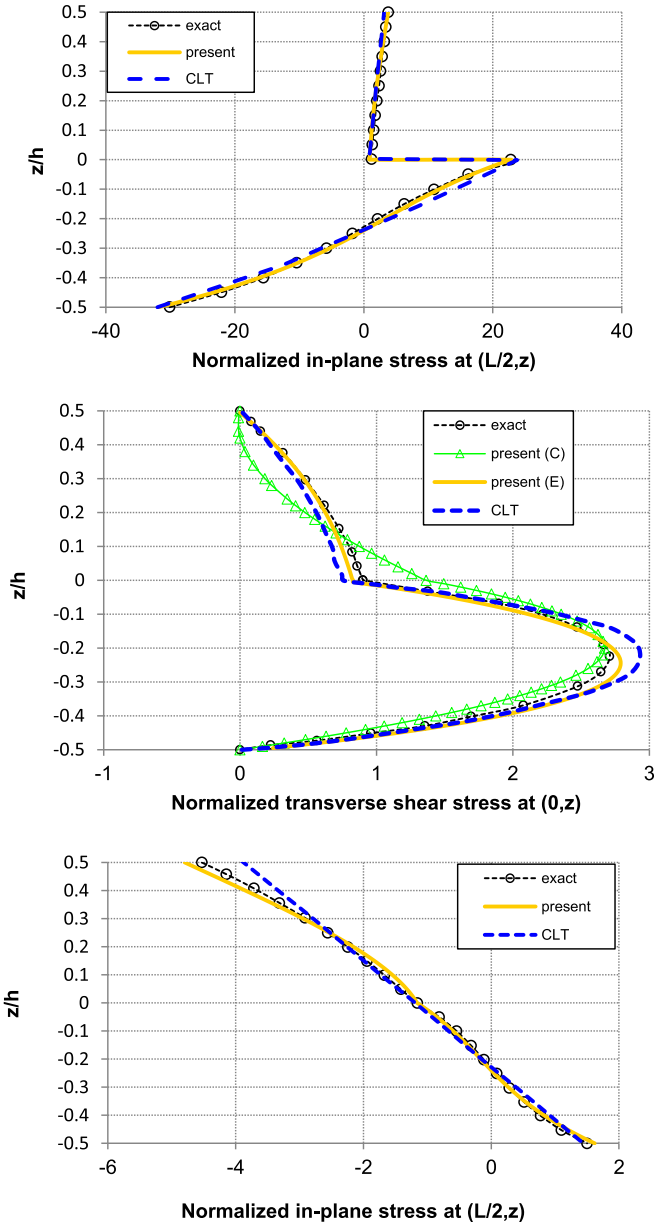

Fig. 5. Through-the-thickness distribution of $\bar{\sigma}_{11}, \bar{\sigma}_{13}$ and $\bar{u}_1$ for the simply supported two-layer beam ($S = 4$).

Table 13
$u_3(L,0)$ of the cantilever $[90^\circ/0^\circ/0^\circ/90^\circ]$ beam for different S ratios.

S	$w(L,0)$		
	ABAQUS	Present	Difference (%)
4	-4.5829×10^{-6}	-4.4778×10^{-6}	2.35
10	-5.7154×10^{-5}	-5.6928×10^{-5}	0.40
50	-6.8017×10^{-3}	-6.8105×10^{-3}	0.13

correlated very well with ABAQUS results. These results show that the present isogeometric formulation is suitable for predicting behaviors of the composite laminated beams with different boundary conditions.

4.1.6. A sandwich beam with a soft core

A simply supported thick sandwich beam with a soft core with the following geometric parameters is considered:

$$L=10m,\quad b=1m,\quad h_f=0.1h,\quad h_c=0.8h,\quad S=4$$

where, the subscripts "f" and "c' stand for the face sheets and core, respectively. The core is made of a DivingH60 Cell with the following material properties:

$$E_c=56MPa,\quad \rho_c=60kg\Big/m^3,\quad \nu_c=0.27$$

The face sheets are made of graphite-epoxy with the following material properties:

$$(E_{11},E_{22},E_{33},G_{12},G_{13},G_{23})=(131.1,6.9,6.9,3.588,3.088,2.3322)\ GPa$$

$$(\nu_{12},\nu_{13},\nu_{23})=(0.32,0.32,0.49),\quad \rho_f=1000kg\Big/m^3$$

Therefore, ratio of the Young's modulus of the face sheets to Young's modulus of the core is very high. The sandwich beam is subjected to a uniform pressure $p_0=-1000N/m^2$.

The through-the-thickness distribution of the transverse displacement, in-plane and transverse shear stresses are depicted in Fig. 7. The present results are compared with 3D FE results of a commercial code (ABAQUS). The proposed NURBS-based isogeometric approach predicts the transverse displacement of the sandwich beam with an error rate of less than 2%. It may be readily noticed that the in-plane and transverse shear stresses calculated from the equilibrium equations are in an excellent agreement with the 3D finite element results. These results confirm the effectiveness of the present formulation for the bending analysis of sandwich beams with high face to core stiffness ratios.

4.2. Free vibration analysis

In this section, the IGA approach is assessed for free vibration analysis. The accuracy of the method is discussed. A convergence study and the influence of the parameterization are first addressed. Then, different symmetric, anti-symmetric and sandwich structures are considered.

4.2.1. Properties of the isogeometric approach

A simply-supported composite cross-ply $[90^\circ/0^\circ/0^\circ/90^\circ]$ beam with a length to thickness ratio of $S=5$ (severe case) is carried out. The beam is made of a material with the following properties:

$$(E_L,E_T,G_{LT},G_{TT})=(181,10.3,7.17,2.87)GPa,$$
$$(\nu_{LT},\nu_{TT})=(0.25,0.33),\quad \rho=1578kg\Big/m^3$$

These results are presented in terms of the following non-dimensional natural frequency: $\overline{\omega}=\omega LS(\rho/E_T)^{1/2}$

A convergence study is first presented in Table 14 considering different number of control points and various orders of NURBS basis functions, using linear parameterization and one element (k = n + 1). In this table, the order of the employed basis functions is higher than 5. However, it is seen from the first three columns of this table that the isogeometric formulation cannot predict the higher modes of the composite beams accurately. This problem is due to the insufficiency in the number of employed control points.

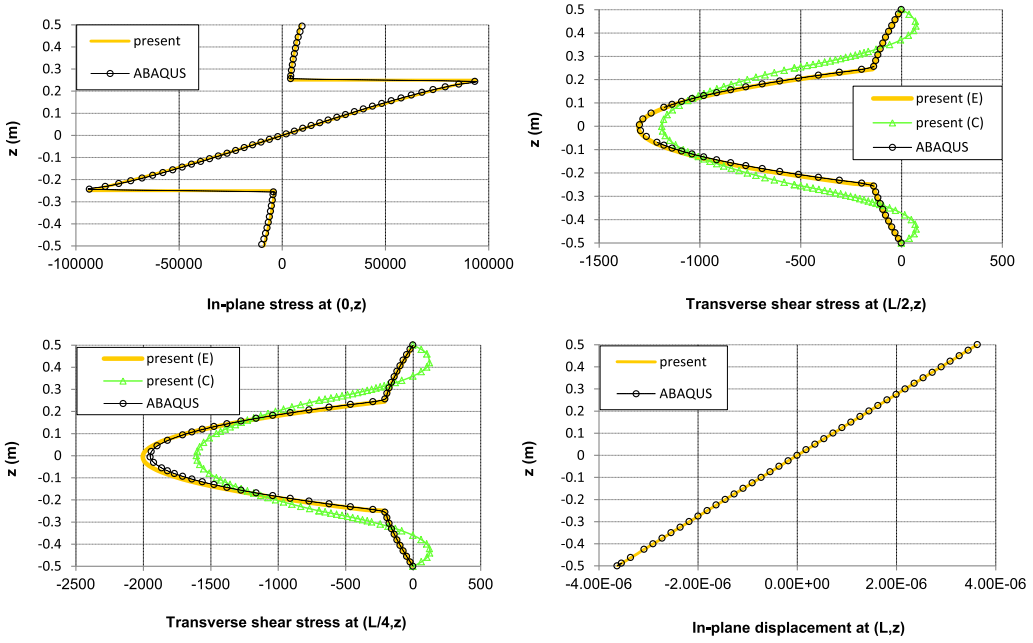

Fig. 6. Through-the-thickness distribution of $\sigma_{11}(N/m^2)$, $\sigma_{13}(N/m^2)$ and u_1 (m) at different sections of the clamped $[90^\circ/0^\circ/0^\circ/90^\circ]$ beam with $S=10$.

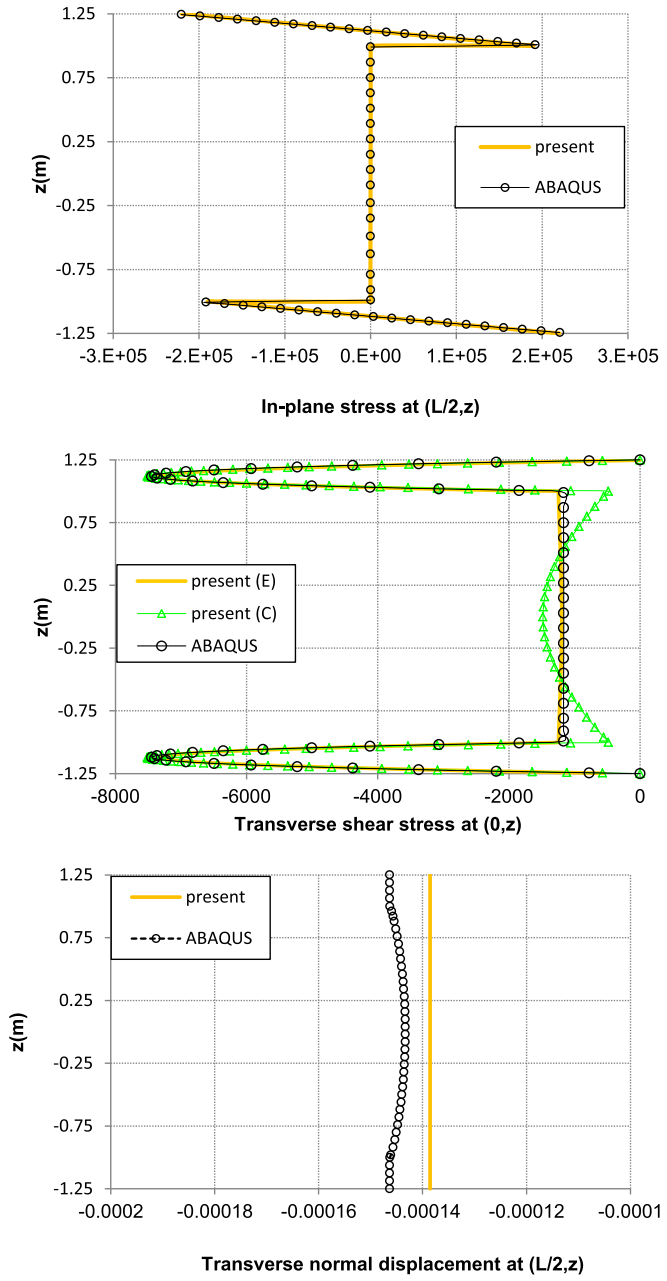

Fig. 7. Variations of $\sigma_{11}(N/m^2)$, $\sigma_{13}(N/m^2)$ and u_3 (m) along the thickness direction for the soft-core sandwich beam ($S = 4$).

Table 14
Mesh convergence study for the four-layer $[0°/90°/90°/0°]$ beam using the different order of NURBS basis functions and control points/nodes- (1 element; k = n + 1)- ($S = 5$).

Mode type	Number of control points/nodes (order of basis function)						
	6 (6)	7 (7)	8 (8)	9 (9)	10 (10)	13 (13)	16 (16)
Bend	7.431	6.815	6.815	6.815	6.815	6.815	6.815
Bend	17.340	16.549	16.541	16.541	16.541	16.541	16.541
Bend	33.826	26.844	26.789	26.719	26.718	26.717	26.717
Bend	47.808	43.201	37.746	37.601	37.294	37.281	37.281
sh	43.803	43.803	43.803	43.803	43.803	43.803	43.803
Bend	–	61.013	59.420	49.296	49.031	48.089	48.088
Bend	–	–	79.838	78.234	61.589	59.186	59.035
No. dofs	24	28	32	36	40	52	64

Table 15
Mesh convergence study for the four-layer $[0°/90°/90°/0°]$ beam using the different order of NURBS basis functions; n = 15- ($S = 5$).

Mode type	Non-dimensional natural frequencies				
	k = 2	k = 3	k = 4	k = 5	k = 16
Bend	5.086	6.817	6.815	6.815	6.815
Bend	11.975	16.595	16.541	16.541	16.541
Bend	18.764	27.101	26.723	26.717	26.717
Bend	25.577	38.855	37.330	37.281	37.281
sh	43.803	43.803	43.803	43.803	43.803
Bend	32.468	52.849	48.357	48.088	48.088
Bend	39.451	70.939	60.152	59.035	59.035
No. dofs	64	64	64	64	64
No. elements	15	14	13	12	1

The last three columns of Table 14 show that with the increase of the number of control points, the accuracy is improved. It can be concluded from these results that a merely use of high order NURBS basis functions does not lead to accurate results. For an accurate free vibration isogeometric analysis, the use of sufficient number of control points is essential. Additional numerical results are given in Tables 15 and 16. Table 15 shows results of the convergence study considering different orders of NURBS basis functions and 16 control points/nodes (n = 15). It is seen from this table that the use of the NURBS basis functions of order 4 (k = 5) with 16 control points is enough for a vibration analysis. Moreover, results of the convergence study considering different number of control points and NURBS basis functions of order 4 are also given in Table 16. It can be observed that the use of more than 16 control points does not change the first seven natural frequencies of the symmetric laminated beam significantly. Based on the convergence study, all the subsequent results are obtained using order 4 and 16 control points (n = 15, k = 5, 64 dofs).

Then, the effect of different parameterizations on the vibration results is studied in Tables 17 and 18. The cross-ply $[90°/0°/0°/90°]$ beam is modelized using quartic NURBS basis functions with different sets of control points. Data of different locations of control points are given in Table 17. "Case A" leads to a linear parameterization while the other cases lead to nonlinear parameterizations. The obtained natural frequencies with the associated error rate are shown in Table 18. Similar to the static tests, the linear parameterization (case A) and the nonlinear parameterization with equally spaced control points (case D) lead to more accurate results. Note that the error rate on the fundamental mode remains low regardless of the case. The influence of the local modification of the control points is greater for the higher mode. Thus, the subsequent isogeometric results are calculated using the linear parameterization.

Table 16
Results of the convergence study for the non-dimensional natural frequencies of the four-layer $[0°/90°/90°/0°]$ beam using the different number of control points/nodes; k = 5- ($S = 5$).

Mode type	Number of control points/nodes			
	5	8	16	25
Bend	6.816	6.815	6.815	6.815
Bend	17.288	16.544	16.541	16.541
Bend	30.175	26.901	26.717	26.717
Bend	–	38.959	37.281	37.281
sh	43.802	43.802	43.803	43.803
Bend	–	47.868	48.088	48.089
Bend	–	60.958	59.035	59.038
No. dofs	20	32	64	100
No. elements	1	4	12	21

Table 17
The coordinates of different sets of control points employed in the vibration tests.

i	$\bar{x}_i$			
1	0	0	0	0
2	$L/48$	$0.07L$	$0.07L$	$0.07L$
3	$3L/48$	$0.13L$	$0.13L$	$0.13L$
4	$6L/48$	$0.23L$	$0.20L$	$0.20L$
5	$10L/48$	$0.30L$	$0.27L$	$0.27L$
6	$14L/48$	$0.37L$	$0.33L$	$0.33L$
7	$18L/48$	$0.40L$	$0.40L$	$0.40L$
8	$22L/48$	$0.47L$	$0.47L$	$0.47L$
9	$26L/48$	$0.53L$	$0.53L$	$0.53L$
10	$30L/48$	$0.60L$	$0.65L$	$0.60L$
11	$34L/48$	$0.67L$	$0.72L$	$0.67L$
12	$38L/48$	$0.73L$	$0.79L$	$0.73L$
13	$42L/48$	$0.83L$	$0.80L$	$0.80L$
14	$45L/48$	$0.90L$	$0.87L$	$0.87L$
15	$47L/48$	$0.97L$	$0.93L$	$0.93L$
16	L	L	L	L
	Case A	Case B	Case C	Case D

4.2.2. Free vibration of symmetric lay-up composite beam

Free vibration analysis of a simply supported composite cross-ply $[0^\circ/90^\circ/90^\circ/0^\circ]$ beam with a length to thickness ratios of $S = 5, 10$ and 20 is carried out. The same material as in Section 4.2.1 is used. Table 19 presents the computed natural frequencies. In this table, the mode shapes are precised as: bend, sh, t/c, for bending, shear and axial traction/compression mode respectively. The mode shapes of the thick beam (S=5) are shown in Fig. 8. Description of the modes is given in Table 19. For comparison purposes, results of the refined sinus finite element model (Vidal and Polit, 2008) and 2D finite element (ANSYS) are given. Table 19 shows that results of the proposed isogeometric formulation agree well with the ANSYS values. The present isogeometric formulation predicts the first fundamental natural frequency of the thick to thin beams with the maximal error rate of 0.1%. The discrepancy in the prediction of the first seven non-dimensional natural frequencies of the thick to thin beams is less than 2.1%. It is also seen from Table 19 that the accuracy of the present isogeometric formulation in the prediction of non-dimensional natural frequencies is slightly better than the refined sinus finite element model. This phenomenon is probably due to the fact that the NURBS basic functions can provide higher order continuity on the displacement field.

4.2.3. Free vibration of anti-symmetric lay-up composite beam

In this example, free vibration analysis of a simply supported composite beam is carried out. Geometry and material properties of the laminated composite beam are the same as those of the previous section. Here, the anti-symmetric lay-up $[0^\circ/90^\circ]$ is considered. The non-dimensional natural frequencies of the composite beams are summarized in Table 20 for three values of length-to-thickness ratios $S = 5$, $S = 10$ and$S = 20$. Similar to the composite beams with symmetric lay-up, the results obtained from the present NURBS-based isogeometric formulation are very close to the reference values. Table 20 shows that the present isogeometric formulation yields more accurate results than refined sinus finite element model in all cases. The maximum error rate is 3.72%.

Table 19
Non-dimensional natural frequencies of the four-layer $[0^\circ/90^\circ/90^\circ/0^\circ]$ beam.

S	Non-dimensional natural frequencies					
		Present	Error (%)	SinRef-c	Error (%)	ANSYS
5	Bend	6.81	0.1	6.81	0.2	6.81
	Bend	16.54	0.1	16.45	0.1	16.52
	Bend	26.72	0.0	26.73	0.04	26.72
	Bend	37.28	0.1	37.32	0.02	37.33
	sh	43.80	0.0	43.80	0.01	43.79
	Bend	48.09	0.2	48.18	0.4	48.17
	Bend	59.04	0.1	59.26	0.2	59.11
10	Bend	9.35	0.1	9.36	0.1	9.34
	Bend	27.26	0.1	27.25	0.1	27.24
	Bend	46.49	0.0	46.53	0.1	46.47
	Bend	66.16	0.1	66.25	0.1	66.19
	Bend	86.29	0.2	86.51	0.1	86.43
	t/c	95.74	2.1	95.90	2.2	93.78
	Bend	106.87	0.3	107.38	0.1	107.20
20	Bend	10.64	0.0	10.65	0.1	10.64
	Bend	37.40	0.0	37.45	0.1	37.40
	Bend	71.82	0.0	71.94	0.1	71.85
	Bend	109.04	0.1	109.30	0.1	109.15
	Bend	147.26	0.2	147.83	0.2	147.54
	Bend	185.98	0.3	187.19	0.3	186.53
	t/c	191.47	0.5	191.81	0.6	190.52

4.2.4. Free vibration of sandwich beam

In this section, a three-layer simply supported sandwich beam with S = 10 and 20 is considered. Thickness of each face sheet is 0.1 h and thickness of the core is 0.8 h. The face sheets are made of graphite-epoxy with the following material properties:

$$(E_{11}, E_{22}, E_{33}, G_{12}, G_{13}, G_{23}) = (131.1, 6.9, 6.9, 3.588, 3.088, 2.3322)\ GPa$$

The material properties of the core are:

$$(E_{11}, E_{22}, E_{33}, G_{12}, G_{13}, G_{23}) = (0.2208, 0.2001, 2760, 16.56, 545.1, 455.4)MPa$$

Table 18
The effect of different parameterization on the non-dimensional natural frequencies; four-layer $[0^\circ/90^\circ/90^\circ/0^\circ]$ beam with S = 5; (n = 15, k = 5).

Mode type	Non-dimensional natural frequencies							
	Case A	Error (%)	Case B	Error (%)	Case C	Error (%)	Case D	Error (%)
Bend	6.815	0.07	6.820	0.15	6.824	0.21	6.815	0.07
Bend	16.541	0.13	16.575	0.33	16.616	0.58	16.546	0.16
Bend	26.717	0.01	26.832	0.42	27.059	1.27	26.742	0.08
Bend	37.281	0.13	37.608	0.74	37.921	1.58	37.358	0.08
sh	43.803	0.03	43.803	0.03	43.803	0.03	43.803	0.03
Bend	48.088	0.17	48.276	0.22	48.360	0.39	48.305	0.28
Bend	59.035	0.13	60.702	2.69	62.611	5.92	59.710	1.02

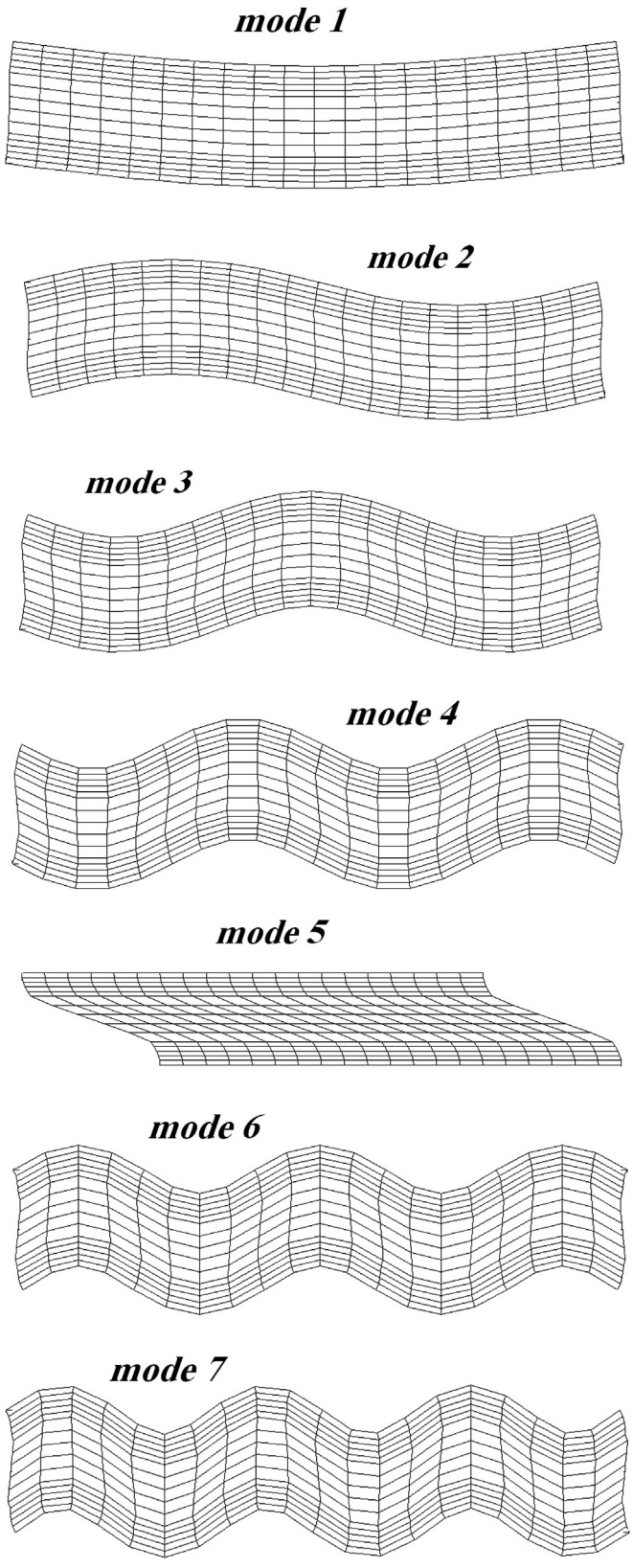

Fig. 8. Mode shapes of the four-layer $[0^\circ/90^\circ/90^\circ/0^\circ]$ beam with $S = 5$ (description of the modes are given in Table 19).

Table 20
Non-dimensional natural frequencies of the anti-symmetric $[0^\circ/90^\circ]$ beam.

S		Non-dimensional natural frequencies				
		Present	Error (%)	SinRef-c	Error (%)	ANSYS
5	Bend	4.78	0.2	4.78	0.2	4.77
	Bend	14.70	0.6	14.71	0.6	14.61
	Bend	25.85	1.8	25.87	1.8	25.40
	t/c	35.53	0.3	35.56	0.4	35.42
	Bend	37.36	3.7	37.42	4	36.02
	sh	48.53	0.0	48.52	0.	48.52
10	Bend	5.29	0.0	5.29	0.1	5.29
	Bend	19.12	0.0	19.14	0.1	19.12
	Bend	37.80	0.1	37.87	0.2	37.77
	Bend	58.79	0.3	58.97	0.6	58.60
	Bend	80.83	0.8	81.26	1	80.22
	t/c	88.52	0.1	88.65	0.2	88.44
20	Bend	5.45	0.0	5.45	0.1	5.45
	Bend	21.17	0.1	21.20	0.1	21.18
	Bend	45.51	0.1	45.62	0.1	45.55
	Bend	76.46	0.2	76.81	0.3	76.59
	Bend	112.19	0.2	113.11	0.6	112.40
	Bend	151.21	0.2	153.29	1	151.48
	t/c	187.93	0.0	188.26	0.2	187.89

$$(\nu_{12}, \nu_{13}, \nu_{23}) = (0.99, 0.00003, 0.00003), \quad \rho_c = 70kg/m^3$$

Similar to the previous example, results are presented in terms of the following non-dimensional natural frequency:

$$\overline{\omega} = \omega LS\left(\rho_f / E_0\right)^{1/2}$$

where $E_0 = 6.9GPa$. The dimensionless natural frequencies of the sandwich beam are given in Table 21. The numerical results are compared with results of the refined sinus finite element model (Vidal and Polit, 2008), 2D finite element (ANSYS) and exact 2D solutions (Kapuria et al., 2004). It can be inferred from Table 21 that the proposed isogeometric formulation yields accurate results in all cases. The present formulation is able to predict the first six non-dimensional frequencies of the thick and relatively thick sandwich beams with a maximum difference of 4.2%. In case of thin beam, the error is less than 2.8%. Note also that the results obtained

Table 21
Non-dimensional natural frequencies of the sandwich beam.

S		Non-dimensional natural frequencies					
		Present	Error (%)	SinRef-c	Error (%)	ANSYS	Exact 2D
5	Bend	8.04	2.8	8.04	2.7	7.82	7.82
	Bend	17.86	3.4	17.86	3.3	17.28	17.27
	Bend	27.87	3.5	27.88	3.5	26.93	26.90
	sh	34.22	2.5	34.22	2.4	33.40	
	Bend	38.32	3.5	38.35	3.6	37.01	36.93
	Bend	49.20	3.5	49.31	3.6	47.55	47.39
	t/c	60.46	4.2	60.68	4.5	58.02	–
	Bend	60.52	3.4	60.72	3.7	58.51	58.22
10	Bend	12.44	1.7	12.45	1.7	12.23	12.23
	Bend	32.14	2.7	32.16	2.7	31.30	31.29
	Bend	51.80	3.1	51.82	3.1	50.26	50.21
	Bend	71.42	3.2	71.48	3.2	69.21	68.09
	Bend	91.27	3.2	91.43	3.4	88.41	88.18
	Bend	111.50	3.2	111.91	3.5	108.02	107.61
	t/c	121.04	0.8	121.36	1.1	120.03	–
20	Bend	15.48	0.6	15.51	0.8	15.38	15.38
	Bend	49.75	1.6	49.82	1.7	48.98	48.94
	Bend	88.91	2.2	89.03	2.3	87.01	86.90
	Bend	167.98	2.7	168.41	2.9	163.58	163.12
	Bend	207.20	2.8	208.08	3.1	201.64	200.87
	t/c	242.08	0.2	242.73	0.4	241.61	–

for the thick case can be improved by considering the influence of the transverse normal deformation.

The above obtained numerical results prove the efficiency of the proposed NURBS-based isogeometric formulation for the free vibration analysis of laminated composite and sandwich beams with wide range of length to thickness ratios.

5. Conclusions

In this paper, a NURBS-based isogeometric approach is developed for the static and free vibration analysis of laminated composite and sandwich beams. The employed kinematics is based on a refined sinus model. All displacement and transverse shear stress continuities are ensured at layer interfaces between the layers as well as the free boundary conditions on the top and bottom of the beam. The number of the mechanical unknowns remains low and is independent of the number of layers. In order to assess the accuracy of the proposed isogeometric formulation for static and dynamic analyses of laminated beams, comparisons have been made with results obtained from the 2D or 3D finite element (ANSYS and ABAQUS) analyses and other previous published results. To this purpose, various static and dynamic tests with different geometric parameters, stacking sequences and boundary conditions are considered. Accurate results have been found for static bending, natural frequencies and mode shapes. It has been proved that the convergence rate of the present isogeometric formulation is very high. It has also been shown that this approach is free of shear locking for $k > 3$. For $k = 3$, the shear locking phenomenon can be avoided using the field compatibility condition. Due to inherent advantages, e.g. preserving exact geometries and providing the smoothness of field variable approximations with arbitrary continuity order, it seems that the present isogeometric analysis can provide an efficient alternative method to the finite elements analysis of laminated composite and sandwich beam structures.

Further works are pointed towards curved beam developments and axisymetric approaches.

References

Alibeigloo, A., Madoliat, R., 2009. Static analysis of cross-ply laminated plates with integrated surface piezoelectric layers using differential quadrature. Compos. Struct. 88, 342–353.

Ambartsumian, S.A., 1969. Theory of Anisotropic Plates. Translated from Russian by Cheron T and Edited by Ashton JE. Tech. Pub. Co.

Barbero, E.J., Reddy, J.N., Teply, J., 1990. An accurate determination of stresses in thick laminates using a generalized plate theory. Int. J. Numer. Meth. Eng. 29, 1–14.

Bazilevs, Y., Hughes, T.J.R., 2008. NURBS-based isogeometric analysis for the computation of flows about rotating components. Comput. Struct. 43, 143–150.

Bazilevs, Y., Calo, V.M., Hughes, T.J.R., Zhang, Y., 2008. Isogeometric fluid-structure interaction: theory, algorithms and computations. Comput. Struct. 43, 3–37.

Beheshti-Aval, S.B., Lezgy-Nazargah, M., 2010. A finite element model for composite beams with piezoelectric layers using a sinus model. J. Mech. 26 (2), 249–258.

Beheshti-Aval, S.B., Lezgy-Nazargah, M., 2012. A coupled refined high-order global-local theory and finite element model for static electromechanical response of smart multilayered/sandwich beams. Arch. Appl. Mech. 82 (12), 1709–1752.

Beheshti-Aval, S.B., Lezgy-Nazargah, M., 2013. Coupled refined layerwise theory for dynamic free and forced response of piezoelectric laminated composite and sandwich beams. Meccanica 48 (6), 1479–1500.

Beheshti-Aval, S.B., Lezgy-Nazargah, M., Vidal, P., Polit, O., 2011. A refined sinus finite element model for the analysis of piezoelectric laminated beams. J. Intell. Mater. Syst. Struct. 22, 203–219.

Beheshti-Aval, S.B., Shahvaghar-Asl, S., Lezgy-Nazargah, M., Noori, M., 2013. A finite element model based on coupled refined high-order global-local theory for static analysis of electromechanical embedded shear-mode piezoelectric sandwich composite beams with various widths. Thin Walled Struct. 72, 139–163.

Benson, D.J., Bazilevs, Y., Hsu, M.C., Hughes, T.J.R., 2010. Isogeometric shell analysis: the Reissner–Mindlin shell. Comput. Methods Appl. Mech. Eng. 199 (5–8), 276–289.

Bui, Q.T., Nguyen, N.M., Zhang, C.h, 2011. An efficient meshfree method for vibration analysis of laminated composite plates. Comput. Mech. 48, 175–193.

Carrera, E., 1999. A study of transverse normal stress effects on vibration of multilayered plates and shells. J. Sound. Vibr 225, 803–829.

Carrera, E., 2000. Single-layer vs multi-layers plate modeling on the basis of Reissner's mixed theorem. AIAA J. 38, 342–343.

Carrera, E., Brischetto, S.A., 2009. Survey with numerical assessment of classical and refined theories for the analysis of sandwich plates. Appl. Mech. Rev. 62, 1–17.

Chen, C.C., Liew, K.M., Lim, C.W., Kitipornchai, S., 1997. Vibration analysis of symmetrically laminated thick rectangular plates using the higher-order theory and p-Ritz method. J. Acoust. Soc. Am. 102, 1600–1611.

Cottrell, J.A., Reali, A., Bazilevs, Y., Hughes, T.J.R., 2006. Isogeometric analysis of structural vibrations. Comput. Methods Appl. Mech. Eng. 195, 5257–5296.

Dau, F., Polit, O., Touratier, M., 2004. An efficient C^1 finite element with continuity requirements for multilayered/sandwich shell structures. Comput. Struct. 82, 1889–1899.

Echter, R., Bischoff, M., 2010. Numerical efficiency, locking and unlocking of NURBS finite elements. Comput. Methods Appl. Mech. Eng. 199, 374–382.

Elguedj, T., Bazilevs, Y., Calo, V., Hughes, T.J.R., 2008. B and F projection methods for nearly incompressible linear and non-linear elasticity and plasticity using higher order NURBS elements. Comput. Methods Appl. Mech. Eng. 197, 2732–2762.

Hu, X.X., Sakiyama, T., Lim, C.W., Xiong, Y., Matsuda, H., Morita, C., 2004. Vibration of angle-ply laminated plates with twist by Rayleigh–Ritz procedure. Comput. Methods Appl. Mech. Eng. 193, 805–823.

Hu, H., Belouettar, S., Potier-Ferry, M., Daya, E.M., 2008. Review and assessment of various theories for modeling sandwich composites. Compos. Struct. 84, 282–292.

Hughes, T.J.R., Cottrell, J.A., Bazilevs, Y., 2005. Isogeometric analysis: CAD, finite elements, NURBS, exact geometry and mesh refinement. Comput. Methods Appl. Mech. Eng. 194, 4135–4195.

Icardi, U., 1998. Eight-noded zig-zag element for deflection and stress analysis of plates with general lay-up. Compos. Part B 29, 425–441.

Icardi, U., 2001. Higher-order zig-zag model for analysis of thick composite beams with inclusion of transverse normal stress and sublaminates approximations. Compos. Part B 32, 343–354.

Icardi, U., 2001. A three-dimensional zig-zag theory for analysis of thick laminated beams. Compos. Struct. 52, 123–135.

Jiarang, F., Jianqiao, Y., 1990. An exact solution for static and dynamics of laminated thick plates with orthotropic layers. Int. J. Solids Struct. 26, 655–662.

Kang, J.H., Shim, H.J., 2004. Exact solutions for the free vibrations of rectangular plates having in-plane moments acting on two opposite simply supported edges. J. Sound. Vib. 273, 933–948.

Kapoor, H., Kapania, R.K., 2012. Geometrically nonlinear NURBS isogeometric finite element analysis of laminated composite plates. Compos. Struct. 94, 3434–3447.

Kapuria, S., Dumir, P.C., Jain, N.K., 2004. Assessment of zigzag theory for static loading, buckling, free and forced response of composite and sandwich beams. Compos. Struct. 64, 317–327.

Leissa, A.W., Kang, J.H., 2002. Exact solutions for vibration and buckling of an SS-C-SS-C rectangular plate loaded by linearly varying in-plane stresses. Int. J. Mech. Sci. 44, 1925–1945.

Lekhnitskii, S.G., 1935. Strength Calculation of Composite Beams. Vestnik inzhen i tekhnikov, No. 9.

Lezgy-Nazargah, M., Shariyat, M., Beheshti-Aval, S.B., 2011. A refined high-order global- local theory for finite element bending and vibration analyses of the laminated composite beams. Acta Mech. 217 (3–4), 219–242.

Lezgy-Nazargah, M., Vidal, P., Polit, O., 2013. An efficient finite element model for static and dynamic analyses of functionally graded piezoelectric beams. Compos. Struct. 104, 71–84.

Li, X., Liu, D., 1997. Generalized laminate theories based on double superposition hypothesis. Int. J. Numer. Methods Eng. 40 (7), 1197–1212.

Liew, K.M., 1996. Solving the vibration of thick symmetric laminates by Reissner/Mindlin plate theory and the p-Ritz method. J. Sound. Vib. 198, 343–360.

Mindlin, R.D., 1951. Influence of rotatory inertia and shear in flexural motions of isotropic elastic plates. ASME J. Appl. Mech. 18, 1031–1036.

Murakami, H., 1984. A laminated beam theory with interlayer slip. J. Appl. Mech. 51, 551–559.

Murakami, H., 1986. Laminated composite plate theory with improved in-plane responses. J. Appl. Mech. 53, 661–666.

Numayr, K.S., Haddad, R.H., Haddad, M.A., 2004. Free vibration of composite plates using the finite difference method. Thin Walled Struct. 42, 399–414.

Pagano, N.J., 1969. Exact solutions for composite laminates in cylindrical bending. J. Compos. Mater. 3, 398–411.

Pagano, N.J., 1970. Exact solutions for rectangular bi-direction composites and sandwich plates. J. Compos. Mater. 4, 20–34.

Pagano, N.J., Hatfield, S.J., 1972. Elastic behavior of multilayered bidirectional composites. AIAA J. 10, 931–933.

Polit, O., Touratier, M., 2000. High-order triangular sandwich plate finite element for linear and non-linear analyses. Comput. Methods Appl. Mech. Eng. 185, 305–324.

Polit, O., Vidal, P., D'Ottavio, M., 2012. Robust C^0 high-order plate finite element for thin to very thick structures: mechanical and thermo-mechanical analysis. Int. J. Numer. Methods Eng. 40, 429–452.

Qian, X., 2010. Isogeometric structural shape optimization. Comput. Methods Appl. Mech. Eng. 199, 2059–2071.

Reddy, J.N., 1987. A generalization of two-dimensional theories of laminated composite plates. Commun. Appl. Numer. Meth. 3 (3), 173–180.

Reddy, J.N., 2004. Mechanics of Laminated Composite Plates and Shells: Theory and Analysis, second ed. CRC Press, Boca Raton.
Reddy, J.N., Barbero, E.J., Teply, J., 1989. A plate bending element based on a generalized laminate plate theory. Int. J. Numer. Meth. Eng. 28, 2275–2292.
Reissner, E., 1945. The effects of transverse shear deformation on the bending of elastic plates. J. Appl. Mech. 12, 69–76.
Reissner, E., 1986. On a mixed variational theorem and on a shear deformable plate theory. Int. J. Numer. Meth. Eng. 23, 193–198.
Ren, J.G., 1986. Bending theory of laminated plates. Compos. Sci. Tech. 27, 225–248.
Ren, J.G., Owen, D.R.J., 1989. Vibration and buckling of laminated plates. Int. J. Solids Struct 25, 95–106.
Robbins Jr., D.H., Reddy, J.N., 1993. Modeling of thick composites using a layerwise laminate theory. Int. J. Numer. Meth. Eng. 36, 655–677.
Rogers, D.F., 2001. An Introduction to NURBS with Historical Perspective. Academic Press, San Diego, CA.
Roh, H.Y., Cho, M., 2004. The application of geometrically exact shell elements to B-spline surfaces. Comput. Methods Appl. Mech. Eng. 193, 2261–2299.
Shariyat, M., 2010. Non-linear dynamic thermo-mechanical buckling analysis of the imperfect sandwich plates based on a generalized three-dimensional high-order global–local plate theory. Compos. Struct. 92, 72–85.
Shariyat, M., 2010. A generalized high-order global–local plate theory for nonlinear bending and buckling analyses of imperfect sandwich plates subjected to thermo-mechanical loads. Compos. Struct. 92, 130–143.
Shariyat, M., 2010. A generalized global–local high-order theory for bending and vibration analyses of sandwich plates subjected to thermo-mechanical loads. Int. J. Mech. Sci. 52, 495–514.
Shojaee, S., Valizadeh, N., Izadpanah, E., Bui, T., Vu, T.V., 2012. Free vibration and buckling analysis of laminated composite plates using the NURBS-based isogeometric finite element method. Compos. Struct. 94 (5), 1677–1693.
Srinivas, S., Rao, A.K., 1970. Bending, vibration and buckling of simply supported thick orthotropic rectangular plates and laminates. Int. J. Solids Struct. 6, 1463–1481.
Srinivas, S., Joga, C.V., Rao, A.K., 1970. An exact analysis for vibration of simply supported homogeneous and laminated thick rectangular plates. J. Sound. Vib. 12, 187–199.
Stavsky, Y., Loewy, R., 1971. On vibrations of heterogeneous orthotropic shells. J. Sound Vibr 15, 235–236.
Thai Chien, H., Nguyen-Xuan, H., Nguyen-Thanh, N., Le, T.H., Nguyen-Thoi, T., Rabczuk, T., 2012. Static, free vibration, and buckling analysis of laminated composite Reissner–Mindlin plates using NURBS-based isogeometric approach. Int. J. Numer. Methods Eng. 91, 571–603.
Thai, C.H., Ferreira, A.J.M., Carrera, E., Nguyen-Xuan, H., 2013. Isogeometric analysis of laminated composite and sandwich plates using a layerwise deformation theory. Compos. Struct. 104, 196–214.
Touratier, M., 1991. An efficient standard plate theory. Int. J. Eng. Sci. 29, 901–916.
Vel, S.S., Batra, R.C., 1999. Analytical solution for rectangular thick laminated plates subjected to arbitrary boundary conditions. AIAA J. 37, 1464–1473.
Venini, P., Mariani, C., 1997. Free vibrations of uncertain composite plates via stochastic Ratleigh–Ritz approach. Compos. Struct. 64, 407–423.
Verhoosel, C.V., Scott, M.A., Hughes, T.J.R., de Borst, R., 2011. An isogeometric analysis approach to gradient damage models. Int. J. Numer. Methods Eng. 86, 115–134.
Vidal, P., Polit, O., 2008. A family of sinus finite elements for the analysis of rectangular laminated beams. Compos. Struct. 84, 56–72.
Vidal, P., Polit, O., 2009. A refined sine-based finite element with transverse normal deformation for the analysis of laminated beams under thermomechanical loads. J. Mech. Mat. Struct. 4, 1127–1155.
Wall, W.A., Frenzel, M.A., Cyron, C., 2008. Full analytical sensitivities in NURBS based isogeometric shape optimization. Comput. Methods Appl. Mech. Eng. 197, 2976–2988.
Wang, Y.Y., Lam, K.Y., Liu, G.R., 2000. Bending analysis of classical symmetric laminated composite plates by the strip element method. Mech. Compos. Mater. Struct. 7, 225–247.
Wang, Y.Y., Lam, K.Y., Liu, G.R., 2001. A strip element method for the transient analysis of symmetric laminated plates. Int. J. Solids Struct. 38, 241–259.
Whitney, J.M., 1969. The effects of transverse shear deformation on the bending of laminated plates. J. Compos. Mater. 3, 534–547.
Whitney, J.M., 1969. The effects of transverse shear deformation on the bending of laminated plates. J. Compos. Mater. 3, 534–547.
Wu, W.X., Shua, C., Wang, C.M., 2008. Mesh-free least-squares-based finite difference method for large amplitude free vibration analysis of arbitrarily shaped thin plates. J. Sound. Vib. 317, 955–974.
Zhang, Y.X., Yang, C.H., 2009. Recent developments in finite element analysis for laminated composite plates. Compos. Struct. 88, 147–157.